Hindawi
Shock and Vibration
Volume 2022, Article ID 1625765, 15 pages
https://doi.org/10.1155/2022/1625765

Research Article

3D Limit Equilibrium Stability Analysis of Concave and Convex Slopes Considering Kinematic Constraints

Xing-Pei Kang,[1] **Ya-Fei Wang**,[1] **Zhan-Rong Zhang**,[1] **Hao Xie**,[1] **and Yun Yang**[2]

[1]*Chinese Railway Si-Yuan Survey and Design Group CO LTD, Wuhan 430063, Hubei Province, China*
[2]*School of Civil Engineering, Central South University, No.22 Shaoshan South Road, Changsha 410075, Hunan Province, China*

Correspondence should be addressed to Yun Yang; 867865420@qq.com

Received 16 May 2022; Revised 29 June 2022; Accepted 4 July 2022; Published 18 August 2022

Academic Editor: He Mingming

In the previous limit equilibrium stability analyses of concave and convex slopes, the kinematic constraints are not considered in the generation of slip surfaces. To tackle this problem, this technical note proposes a method to compute safety factors of concave and convex slopes, combining the simplified Bishop method with an adaptive "point-by-point" technique. Through the adaptive "point-by-point" technique, the failure surfaces of slopes are linked by numerous lines that connect two neighboring discretized points, at which the velocity compatibilities are strictly satisfied. Stress analyses are made for the vertical discretized slices where the lateral pressure on the interface between soil slices is represented by the Rankine active earth pressure. Based on the simplified Bishop method and the strength reduction method, the safety factor and failure surfaces of concave and convex slopes are derived, which are verified by numerical simulations. Comparative outcomes show that the results would be closer to those of numerical simulations if the strength reduction is made for the Rankine active earth pressure on the interface between soil slices. And the proposed discretized slip surface considering kinematic constraints is more consistent with the shear bands by numerical simulation, as compared with the circular arc slip surface. Under homogeneous soil conditions, the proposed discretized slip surface can degenerate into a logarithmic spiral.

1. Introduction

With the popularization of computers, numerical simulation methods become one of the most robust tools for slope stability analyses of slopes. Lorig [4] analyzed the influence of plan geometry, the definition of pore pressure distribution from flow analysis, in situ stresses, and other factors on the stability of concave slope by FLAC3D and pointed out that plane geometry has significant influences on the stability of concave slopes. Cała [5] used finite difference numerical software FLAC3D to analyze the stability of axisymmetric concave and convex slopes under different radius conditions and drew some conclusions. Firstly, the stability of concave slopes is higher than that of convex slopes. Secondly, with the gradual increase of radius, the stability of both concave and convex slopes decreases gradually. Sun et al. [6] proposed a set of diagrams for estimating the stability of homogeneous three-dimensional concave and convex slopes by using displacement finite element software ABAQUS, they concluded that concave slope is more stable than straight slope and the stability of convex slope is worse. At the same time, Sun et al. [6] pointed out that the smaller the relative curvature radius, the more significant the three-dimensional effect of slope and the greater the stability difference between concave and convex slopes. Although the numerical simulation method can get reasonable results of slope stability analysis, there are some weaknesses in practical application, such as being time-consuming and highly dependent on mesh-setting.

The limit equilibrium method has been widely employed as a concise and effective tool to analyze slope stability [7, 8]. The crucial step of the limit equilibrium stability analysis of concave and convex slopes is generating a failure surface in advance. Zhang [9] proposed a practical and straightforward three-dimensional stability analysis method for plane concave slope in which the slip surface was taken to be approximately the surface of an elliptic revolution, satisfying force and moment balances on the unstable body. The

author found that the concave slopes become more stable with the decrease of relative curvature radius R/H. Also, when R/H is small, the slope failure occurs on concave slopes instead of toe failure. Zhang et al. [10] analyzed the effects of curvature radius and top and bottom arch height on the stability of concave slope by using a circular slip surface. The authors found that the slope stability coefficient decreases after increases in the transition stage from flat to concave, and there is an optimal size to get the maximum safety coefficient. Cheng and Lau [11] adopted the simplified Bishop method and simplified Janbu method to study the influence of slope curvature on spherical damage of concave and convex slopes, and they concluded that compared with straight slope, the factor of safety (FS) of concave slopes and convex slopes are larger and smaller, respectively. Although these works predicted accurate enough FSs of concave and convex slopes, curved surfaces are necessary to be assumed for slip surfaces, such as cylindrical [12], spherical [13], and ellipsoidal [14]. More importantly, these postulated slip surfaces may not satisfy the flow law, thus predicting unrealistic FSs.

In this study, a semianalytical model is developed to evaluate the FS of concave and convex slopes based on the limit equilibrium method. Instead of assuming a curve, the slip line in the two-dimensional space can be generated automatically by a forward difference discretization technique. Three-dimensional discretized failure surfaces of concave and convex slopes are generated by rotating the two-dimensional slip line around an axis. Based on Bishop and Rankine's methods, the limit equilibrium formula on soil slices is established, in which the lateral stress on both sides of the soil slice is simplified as the Rankine active earth pressure. The strength reduction method is employed to compute the critical FSs. The correctness of the proposed method is verified by the finite difference software FLAC3D. The advance of the proposed slip curve in the two-dimensional space is highlighted, and whether the reduction of soil parameters in calculating lateral force on slices is necessary is discussed.

2. 3D Limit Equilibrium Analysis of Convex Slope and Concave Slope considering Kinematic Constraints

The conventional two-dimensional analysis approach is the most widely used for slope stability analyses because of advantages such as simple computation and accurate findings. Three-dimensional effects can be ignored when calculating FSs of straight slopes since the lateral pressure among soil coulombs inside slopes are in the same direction. However, because of a circular acting force at the lateral sides (there is an inclination angle between two sides) of soil coulombs, a radial resultant force objectively exists inside the slope body. As a result, the impact of soil lateral pressures on slope stability of concave and convex slopes cannot be overlooked. When the problem domain is reduced to a two-dimensional one, lateral pressures and structural effects are ignored, and thus, the accuracy of stability analysis may be low. This section devotes to developing a rational limit equilibrium model for three-dimensional convex and concave slopes.

2.1. Generation of Failure Surface in the Two-Dimensional Space. The crucial step of the limit equilibrium stability analysis of concave and convex slopes is generating a failure surface in advance, which includes two substeps [10, 11]. As can be seen in Figure 1, a failure curve should be defined in the two-dimensional space, and then the three-dimensional failure surface can be established by rotating a two-dimensional slope model around a certain rotation axis. In the previous stability analyses of concave and convex slopes, a certain type of slip surface, such as circular arc, logarithmic spiral, and so on, is usually assumed. Although the practicability of these slip surfaces has been proved in engineering, the specified type of slip surface cannot reflect the actual failure state of the slope, such as neglecting the kinematic constraints (e.g., the flow rule).

In this section, a forward difference "point-by-point" technique [15–28] is employed to produce the slip line of concave and convex slopes in the two-dimensional space, which allows the kinematic constraint to be accounted for. Several assumptions are made herein: (1) geomaterials should follow the Mohr–Coulomb criterion and the associated flow rule, (2) the slip line passes through slope toe, and (3) potential slip blocks are regarded as rigid bodies and rotate around the rotation center O, as can be seen in Figure 2(a).

As illustrated in Figure 2, the coordinate system is established by taking the slope toe as the coordinate origin (P_0), and the potential slip surface starts from the slope toe and ends at the ground surface. The rotational failure model is considered in this study. The position of the rotation center O is determined by the initial radius r_0 and the initial angle θ_0. In the given coordinate system, the coordinates of rotation center $O(x_0, y_0)$ and slope shoulder $B(x_B, y_B)$ are

$$\begin{cases} x_o = r_o \cos\theta_0, \\ y_o = r_o \sin\theta_0, \end{cases} \begin{cases} x_B = H \cot\beta, \\ y_B = H. \end{cases} \tag{1}$$

The forward difference "point–by-point" process uses a known point on the slip surface to automatically generate the next points on the potential slip surface where the slope toe is adopted as the starting point. Given the coordinates of the point $P_i(x_i, y_i)$, the unit vector $\mathbf{v}_i = (v_{xi}, v_{yi})$ of the velocity at this point can be calculated by the following equation, and the velocity direction is perpendicular to the radial line OP_i:

$$\begin{cases} v_{xi} = -\sin\theta_i, \\ v_{yi} = \cos\theta_i, \end{cases} \tag{2}$$

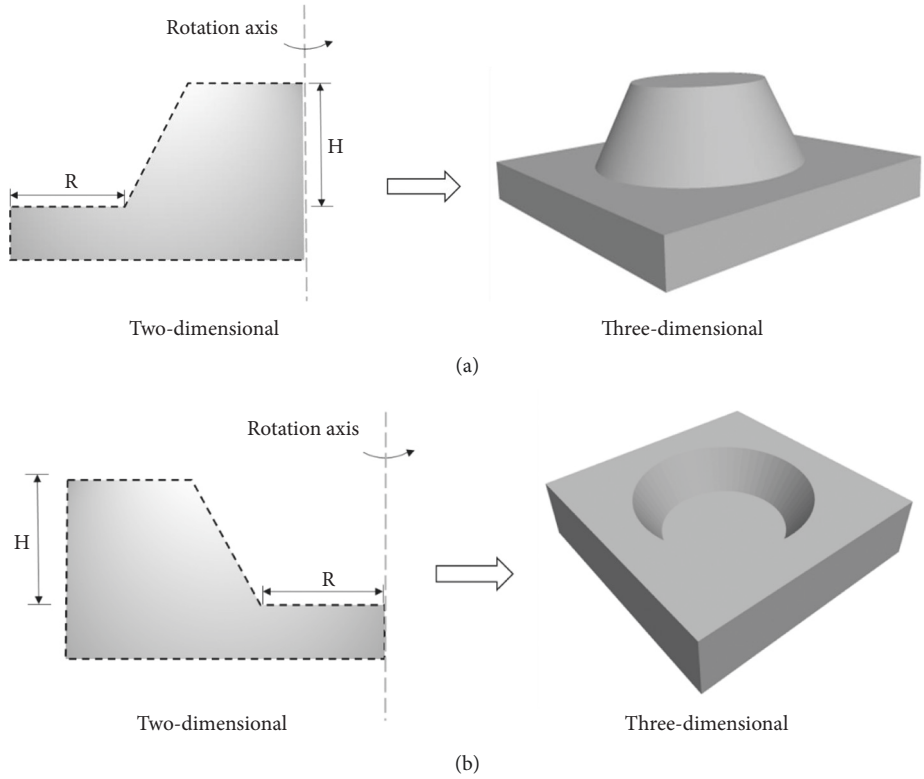

FIGURE 1: The assumed failure mechanisms for the limit equilibrium analyses of concave and convex slopes: (a) concave slope and (b) convex slope.

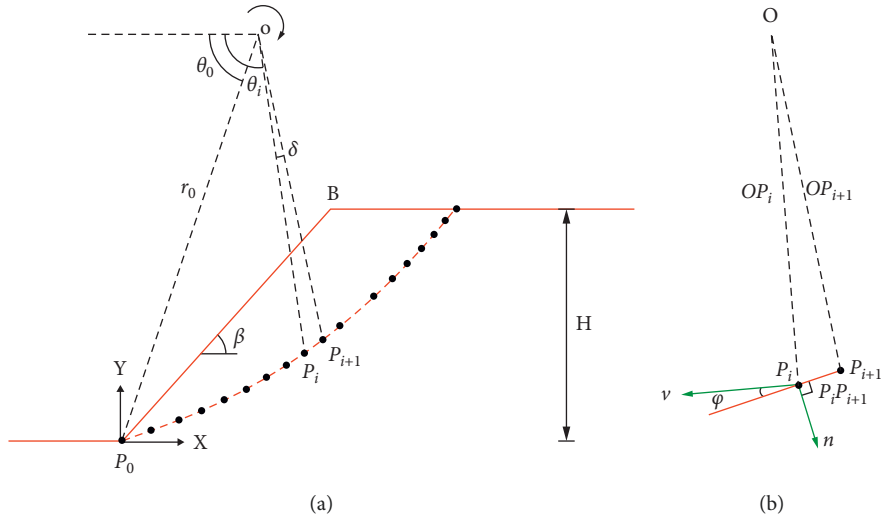

FIGURE 2: Sketch of generation of the two-dimensional failure surface: (a) the process of "point by point" and (b) velocity compatibility at the failure surface.

where θ_i is the angle between the radial line OP_i and a horizontal line passing through point O, as illustrated in Figure 2(a). Next, the coordinates of the unknown point $P_{i+1}(x_{i+1}, y_{i+1})$ can be determined. By obeying the associated flow rule (kinematic constraint), the vector $\mathbf{v}_i$ should make an angle of $\varphi + \pi/2$ with unit outer normal vector $\mathbf{n}_i$ of vector $\mathbf{P}_i\mathbf{P}_{i+1}$, as shown in Figure 2(b), and hence, the following formula can be obtained:

$$\begin{cases} \mathbf{v}_i \cdot \mathbf{n}_i = -\sin\ \varphi, \\ \left|\mathbf{n}_i\right| = 1, \end{cases} \tag{3}$$

$$\mathbf{n}_i \cdot \mathbf{P}_i\mathbf{P}_{i+1} = 0, \tag{4}$$

where φ is the soil friction angle at the point $P_i\ (x_i, y_i)$.

Combining equations (2) and (3), the component of the vector $\mathbf{n}_i$ can be expressed as follows:

$$\begin{cases} n_{xi} = n_{yi} \cot\ \theta_i + \dfrac{\sin\ \varphi}{\sin\ \theta_i}, \\ n_{yi} = \dfrac{-B \pm \sqrt{B^2 - 4AC}}{2A}, \end{cases} \tag{5}$$

where

$$\begin{cases} A = 1 + \ \cot^2\theta_i, \\ B = \dfrac{2\ \sin\ \varphi(y)\cot\ \theta_i}{\sin\ \theta_i}, \\ C = \dfrac{\sin^2\ \varphi(y)}{\sin^2\theta_i} - 1. \end{cases} \tag{6}$$

Then, a unit vector τ_{i+1} is introduced to indicate the direction of the vector $\mathbf{OP}_{i+1}$. So $\mathbf{OP}_{i+1}$ can be expressed as follows:

$$\mathbf{OP}_{i+1} = \lambda_{i+1}\boldsymbol{\tau}_{i+1}, \tag{7}$$

in which

$$\tau_{i+1} = (-\cos\ \theta_{i+1}, -\sin\ \theta_{i+1}), \tag{8}$$

and λ_{i+1} is the length of the vector $\mathbf{OP}_{i+1}$.

Also, the vector $\mathbf{P}_i\mathbf{P}_{i+1}$ can also be expressed as follows:

$$\mathbf{P}_i\mathbf{P}_{i+1} = \mathbf{P}_i\mathbf{O} + \mathbf{OP}_{i+1}. \tag{9}$$

Combining equations (4) and (9), λ_{i+1} can be expressed as follows:

$$\lambda_{i+1} = \frac{n_{xi}(x_0 - x_i) + n_{yi}(y_0 - y_i)}{n_{xi}\cos\ \theta_{i+1} + n_{yi}\sin\ \theta_{i+1}}. \tag{10}$$

Combining equations (7), (8), and (10), the coordinates of the point P_{i+1} can be obtained.

$$\begin{cases} x_{i+1} = x_0 - \lambda_{i+1}\cos\ \theta_{i+1}, \\ y_{i+1} = x_0 - \lambda_{i+1}\cos\ \theta_{i+1}. \end{cases} \tag{11}$$

The whole process of point generation continues until the slip surface reaches the slope ground. Finally, the slip surface is formed by linking up these discrete points. By obeying the normality condition (i.e., kinematic constraints) along the slip surface, the slip line in the two-dimensional space can be generated automatically.

2.2. Limit Equilibrium Analysis. To assess the stability of a concave or convex slope, a 3D model is required. The standard limit equilibrium approach reduces a three-dimensional slope to a two-dimensional planar issue, ignoring the impact of soil lateral pressure on slope stability and resulting in a substantial mistake in the analysis findings. As a result, a two-dimensional model is not suitable for the stability analyses of a concave or convex slope. When conducting a 3D limit equilibrium analysis of a concave slope, it is essential to include the attribute of lateral pressures among neighboring soil columns as well as the impact of the curvature radius of slopes, which are highly dependent on the curvature radii of concave or convex slopes. This section aims at extending the failure surface in the two-dimensional space into a three-dimension problem where the above-mentioned characteristics of concave or convex slopes would be taken into account.

2.2.1. Limit Equilibrium Analysis of Convex Slope. A three-dimensional discrete failure mechanism is obtained by rotating the two-dimensional discrete failure mechanism with an angle $d\theta$ along the rotation axis. Since the stability analysis of convex slopes herein is an axisymmetric problem, the fan-shaped area with an angle $d\theta$ of the convex slope is selected and divided into several vertical strips to conduct the limit equilibrium analyses, as shown in Figure 3. The derivation of the stability calculation formula is based on the simplified Bishop method. And several assumptions are made herein: (a) shear force between adjacent soil slices is in the vertical direction, (b) each soil slice meets vertical force balance, and (c) sliding body satisfies external moment balance.

Soil slice i is selected for conducting force analysis, as illustrated in Figure 3. When $x_{i+1}\tan\ \beta \le H$, the self-weight of a soil slice W_i can be expressed as follows:

$$W_i = \frac{1}{2}\gamma(x_i\tan\ \beta - y_i + x_{i+1}\tan\ \beta - y_{i+1})(x_{i+1} - x_i)r_i d\theta\ . \tag{12}$$

When $x_{i+1}\tan\ \beta > H$, W_i can be expressed as follows:

$$W_i = \frac{1}{2}\gamma(2H - y_i - y_{i+1})(x_{i+1} - x_i)r_i d\theta\ , \tag{13}$$

where γ is the soil unit weight, β is the slope angle; H is the slope height, x_i is the X coordinate of point P_i, y_i is the Y coordinate of point P_i, x_{i+1} is the X coordinate of point P_{i+1}, y_{i+1} is the Y coordinate of point P_{i+1}, and r_i is the horizontal distance from soil slice center to rotation axis and can be written as follows:

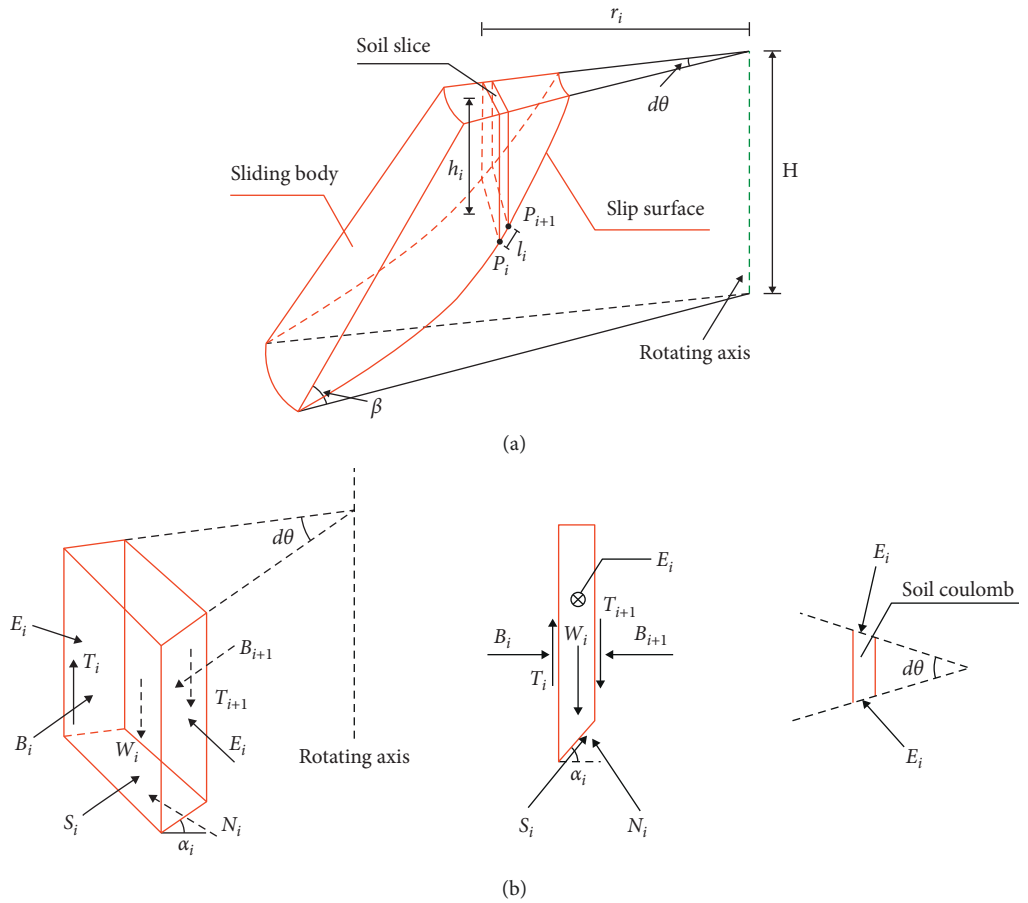

FIGURE 3: Limit equilibrium analyses of convex slopes: (a) fan-shaped part of the convex slope and (b) force analysis of a soil slice in convex slope.

$$r_i = R + \frac{H}{\tan\beta} - \frac{x_i + x_{i+1}}{2}, \tag{14}$$

where R is the rotation radius.

The reduction coefficient (e.g., the FS) of strength parameters is introduced since the strength reduction method would be employed to capture the critical FS of slopes. Then, the antisliding force S_i can be expressed as follows:

$$S_i = \frac{cl_i r_i d\theta}{F_s} + \frac{N_i \tan\varphi}{F_s}, \tag{15}$$

where c is cohesive strength, φ is soil friction angle, N_i is the supporting force at bottom of soil slices, F_s is the reduction coefficient (e.g., FS), l_i is the length of P_iP_{i+1} and reads

$$l_i = \sqrt{(x_i - x_{i+1})^2 + (y_i - y_{i+1})^2}. \tag{16}$$

Since the Bishop method is employed in this study, the shear force T_i and T_{i+1} can be set to zero.

$$W_i - S_i \sin\alpha_i - N_i \cos\alpha_i = 0, \tag{17}$$

where α_i is dip angle at bottom of the soil slice and can be expressed as follows:

$$\alpha_i = \arctan\frac{y_{i+1} - y_i}{x_{i+1} - x_i}. \tag{18}$$

Substituting equations (15) into (17), N_i can be expressed as follows:

$$N_i = \frac{W_i - cl_i r_i \sin\alpha_i d\theta/F_s}{\cos\alpha_i + \sin\alpha_i \tan\varphi/F_s}. \tag{19}$$

The lateral force at both sides of the soil slice can be calculated by Rankine's theory (considered as Rankine active earth force). It is worthy of note that the strength reduction is also made for the calculation of the lateral force where the reduced soil strength parameters, c_r and φ_r, are introduced with $c_r = c/F_s$ and $\varphi_r = \arctan(\tan\varphi/F_s)$. Thereby, the resultant force on one side of the soil slice E_i is as follows:

$$E_i = \left(\frac{1}{2}\gamma h_i^2 K_a - 2c_r h_i \sqrt{K_a} + \frac{2c_r^2}{\gamma}\right)(x_{i+1} - x_i), \tag{20}$$

where h_i is soil slice height and can be expressed as follows:

$$h_i = \frac{1}{2}(x_{i+1} + x_i)\tan\beta - \frac{1}{2}(y_{i+1} + y_i). \tag{21}$$

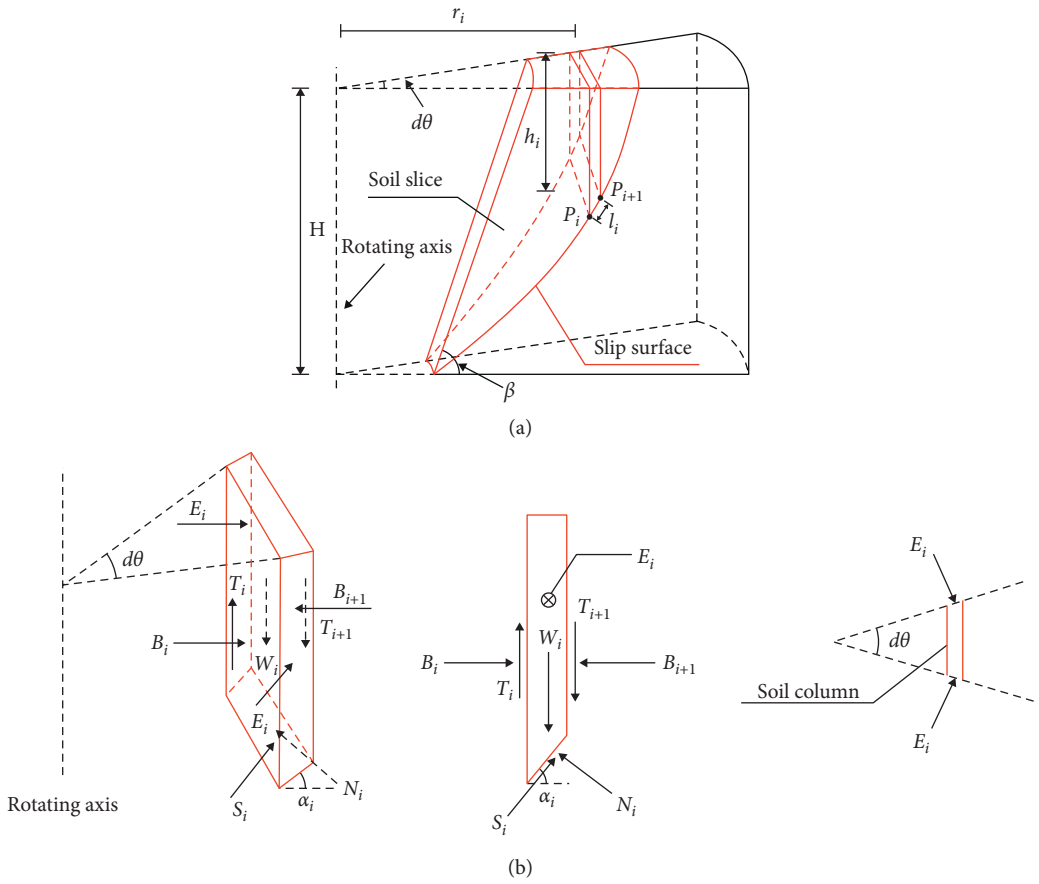

Figure 4: Limit equilibrium analyses of concave slopes: (a) fan-shaped part of the concave slope and (b) force analysis of soil slice in concave slope.

K_a is Rankine's active earth pressure coefficient, and $K_a = \tan^2(45° - \varphi_r/2)$. Rankine's active earth force is located $(h_i - z_0)/3$ above the bottom of the soil slice where z_0 is the critical depth with $z_0 = 2c_r/(\gamma\sqrt{K_a})$.

When the rotation angle $d\theta$ becomes infinitesimal, $\sin d\theta \approx d\theta$. Then, the resultant radial force Q_{Ei} of lateral stress on both sides of the soil slice can be expressed as follows:

$$Q_{Ei} = 2E_i \sin\frac{d\theta}{2} = E_i d\theta = \left(\frac{1}{2}\gamma h_i^2 K_a - 2c_r h_i\sqrt{K_a} + \frac{2c_r^2}{\gamma}\right)(x_{i+1} - x_i)d\theta. \tag{22}$$

Since the sliding body satisfies external moment balance, the following equation can be obtained:

$$\sum W_i X_i + \sum N_i Y_i \sin\alpha_i + \sum Q_{Ei}\left(Y_i - \frac{h_i - z_0}{3}\right) - \sum S_i Y_i \cos\alpha_i - \sum S_i X_i \sin\alpha_i - \sum N_i X_i \cos\alpha_i = 0, \tag{23}$$

where X_i is the horizontal distance from soil slice gravity center to rotation center O and Y_i is the vertical distance from soil slice gravity center to rotation center O. And they can be expressed as follows:

$$\begin{cases} X_i = \dfrac{x_i + x_{i+1}}{2} - x_0, \\ Y_i = y_0 - \dfrac{y_i + y_{i+1}}{2}. \end{cases} \tag{24}$$

It can be found that the F_s is related to the position of the rotation center, (r_0, θ_0) in a polar coordinate system, namely, $F_s = f(r_0, \theta_0)$. Therefore, the critical FS (i.e., the minimum FS) is ultimately calculated by optimizing equation (24), in which r_0 and θ_0 are taken as the optimization variables.

2.2.2. Limit Equilibrium Analysis of Concave Slopes. Since the limit equilibrium analysis of concave slopes is similar to that of convex slopes, only a brief introduction and calculation formulas are presented here. The detailed process can be consulted in Section 2.2.1.

As illustrated in Figure 4(a), a fan-shaped area with an angle dθ of concave slopes is selected and divided into several vertical soil slices. One of the soil slices is selected for balance analysis of forces and moments. Noticeably, unlike

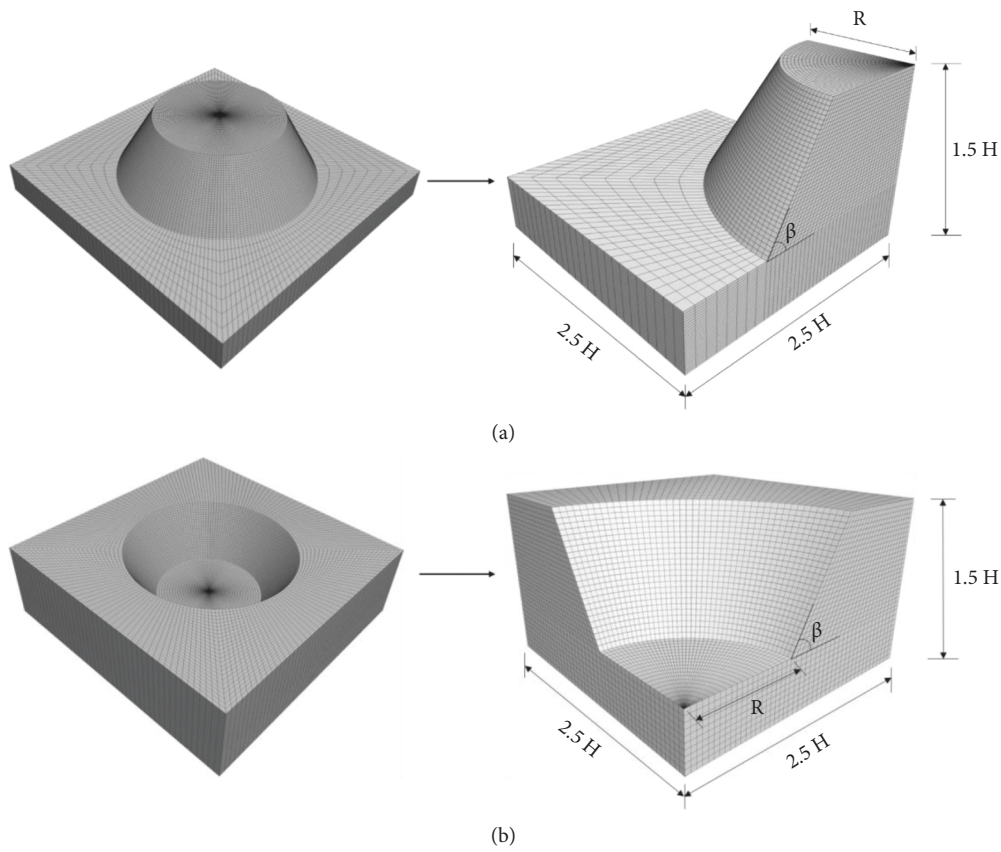

Figure 5: Sketch of finite-difference numerical models: (a) convex slope and (b) concave slope.

convex slopes, the radial component of the lateral stress resultant force Ei is opposite to the slope sliding direction.

The self-weight of the soil slice W_i can be expressed as follows:

$$\begin{cases} W_i = \frac{1}{2}\gamma\left(x_i \tan\beta - y_i + x_{i+1}\tan\beta - y_{i+1}\right)\left(x_{i+1} - x_i\right)r_i d\theta\,, & x_{i+1}\tan\beta \le H, \\ W_i = \frac{1}{2}\gamma\left(2H - y_i - y_{i+1}\right)\left(x_{i+1} - x_i\right)r_i d\theta\,, & x_{i+1}\tan\beta > H, \end{cases} \tag{25}$$

where γ is the soil unit weight, β is the slope angle, H is the slope height, x_i is the X coordinate of point P_i, y_i is the Y coordinate of point P_i, x_{i+1} is the X coordinate of point P_{i+1}, y_{i+1} is the Y coordinate of point P_{i+1}, and r_i is the horizontal distance from soil slice center to rotation axis and can be written as follows:

$$r_i = R + \frac{x_i + x_{i+1}}{2}. \tag{26}$$

The antisliding force S_i can be expressed as follows:

$$S_i = \frac{cl_i r_i d\theta}{F_s} + \frac{N_i \tan\varphi}{F_s}, \tag{27}$$

where c is cohesive strength, φ is soil friction angle, N_i is the supporting force at bottom of soil slices, F_s is the reduction coefficient (e.g., FS), and l_i is the length of P_iP_{i+1} and is calculated by Equation (16).

Considering the force equilibriums in the vertical direction, the normal force N_i at the bottom of the soil slice can be expressed as follows:

$$N_i = \frac{W_i - \left(cl_i r_i \sin\alpha_i d\theta / F_s\right)}{\cos\alpha_i + \left(\sin\alpha_i \tan\varphi / F_s\right)}, \tag{28}$$

in which α_i is calculated by equation (18).

The lateral stress at both sides of the soil slice is also considered as Rankine's active earth force. Combining Rankine active earth force formula with the strength reduction method, the resultant radial force Q_{Ei} of lateral stress on both sides of the soil slice can be expressed as follows:

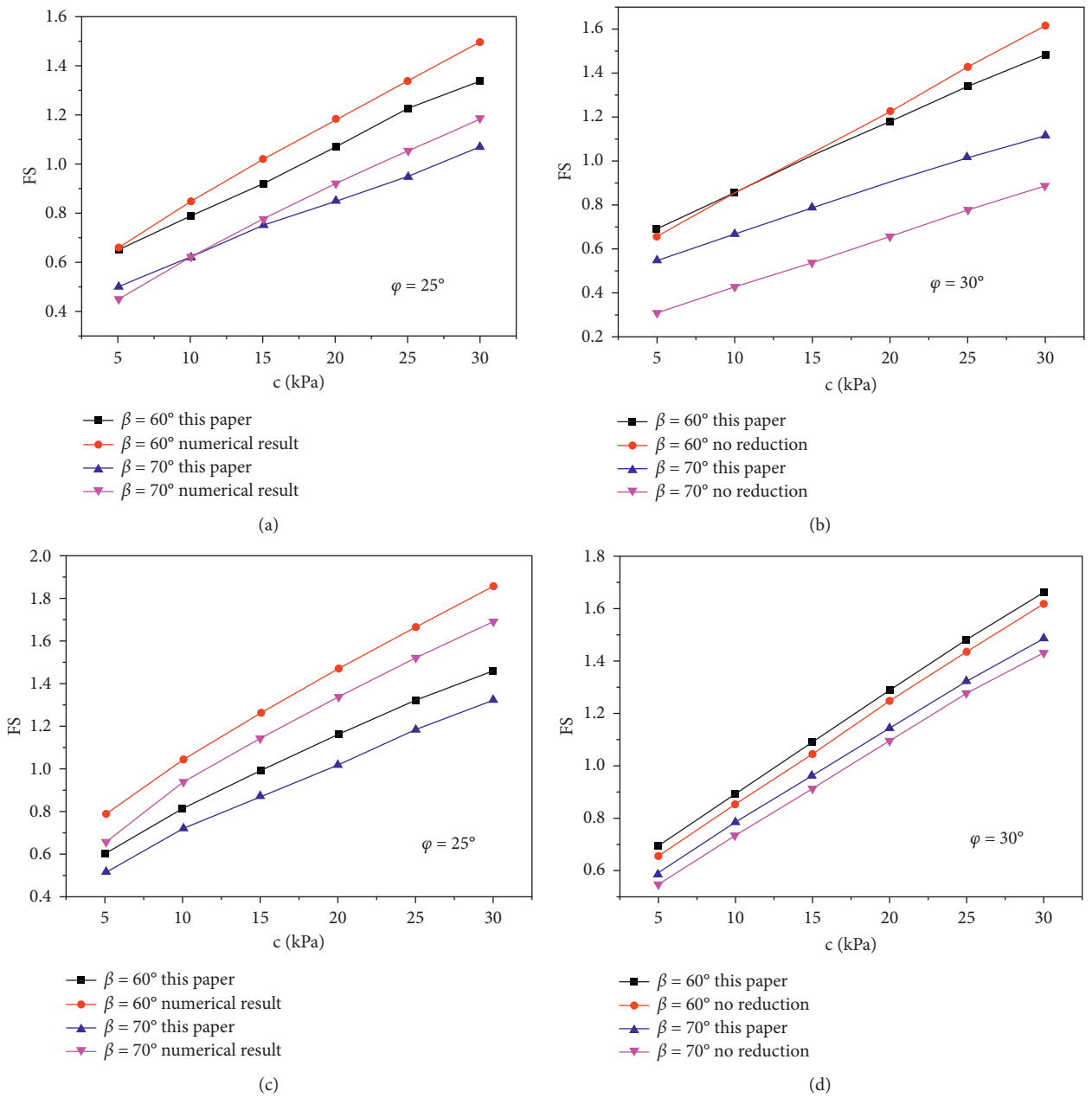

Figure 6: Comparisons with numerical simulations in terms of FSs: (a) and (b) convex slope and (c) and (d) concave slope.

$$Q_{Ei} = \left(\frac{1}{2}\gamma h_i^2 K_a - 2c_r h_i \sqrt{K_a} + \frac{2c_r^2}{\gamma}\right)(x_{i+1} - x_i)d\theta\,, \tag{29}$$

where

$$\begin{cases} h_i = \dfrac{1}{2}(x_{i+1} + x_i)\tan\beta - \dfrac{1}{2}(y_{i+1} + y_i), \\ K_a = \tan^2\left(45^\circ - \dfrac{\varphi_r}{2}\right), \end{cases} \tag{30}$$

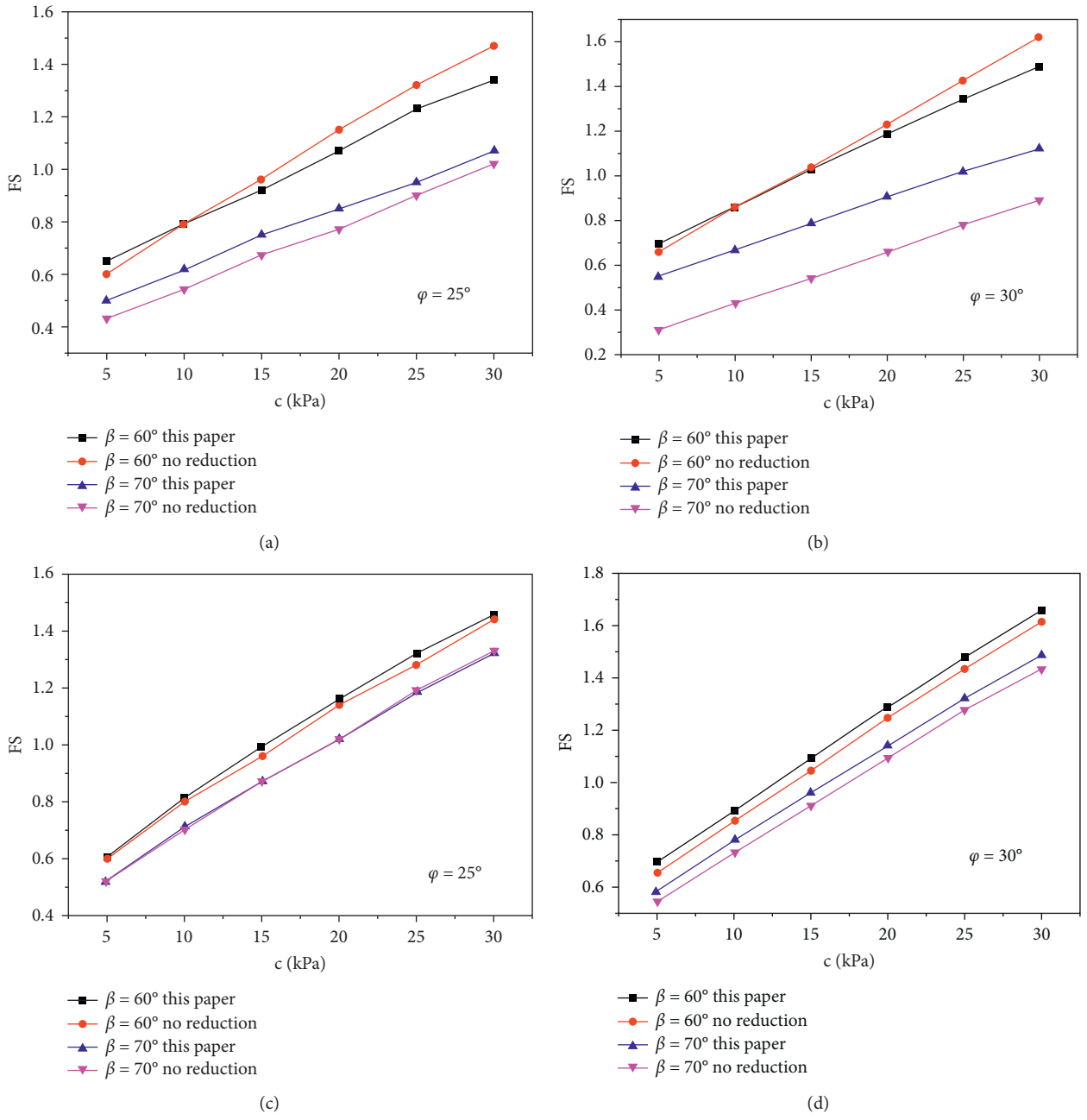

Figure 7: Effect of lateral stress reduction on the FSs: (a) and (b) convex slope and (c) and (d) concave slope.

where Q_{Ei} is located at $(h_i - z_0)/3$ above the bottom of the soil slice and z_0 is the critical depth with $z_0 = 2c_r/(\gamma\sqrt{K_a})$.

By balancing the external moment balance, one can obtain

$$\sum W_i X_i + \sum N_i Y_i \sin \alpha_i - \sum Q_{Ei}\left(Y_i - \frac{h_i - z_0}{3}\right) - \sum S_i Y_i \cos \alpha_i - \sum S_i X_i \sin \alpha_i - \sum N_i X_i \cos \alpha_i = 0, \tag{31}$$

where X_i is the horizontal distance from soil slice gravity center to rotation center O and Y_i is the vertical distance from soil slice gravity center to rotation center O. And they can be expressed by equation (24).

The same with the process of calculating the FS of convex slopes, the F_s is related to the polar coordinates of the rotational center ($r0$, $\theta 0$) in a polar coordinate system, namely, Fs f(r0, $\theta 0$). Therefore, the critical FS (i.e., theminimum FS) is ultimately calculated by optimizing equation (31), in which $r0$ and $\theta 0$ are taken as the optimization variables.

3. Comparisons with Numerical Simulation

In order to verify the proposed method, the FSs calculated by the proposed method are compared with those by numerical software FLAC3D. Because of the axisymmetric nature of the model, only one-quarter of the area is modeled. Figure 5 shows a sketch of the numerical models of a convex slope and a concave slope, and the dimensions of the numerical model are given. For example, a numerical model of a concave slope at a height of 10 m, an inclination of 60°, and a rotation radius of 10 m contains approximately 115,000 zones and 119,554 grid points. Note that this mesh is just for illustration purposes and is not representative of the mesh in all scenarios considered.

In the numerical model, FSs are automatically determined by the strength reduction method. For model boundary conditions, the displacement at the bottom of the model is completely fixed, and the displacements in the normal direction are constrained for the other four vertical boundaries. To characterize the soil masses, a linear elastic-plastic constitutive model (using the Mohr–Coulomb failure criteria) is used. The Young's modulus and Poisson's ratio are set to 15 MPa and 0.3, respectively, in the numerical calculation, which negligibly affects the FS calculated by the strength reduction method [29, 30]. Figure 6 shows the FSs calculated by the proposed method and the numerical simulation, in which the slope height is 10 m, the rotation radius is 10 m, and the soil unit weight is 20 kN/m^3.

In Figure 6(a), the results of the proposed method for all cases are lower than the ones obtained by FLAC3D. It can be seen that the difference between the proposed method and the numerical modeling is within 5%~13% for the case of convex slopes. At the same time, the calculation time of the proposed method is shorter than that of FLAC3D. Usually, using FLAC3D to calculate one case takes nearly 1 hour, while MATLAB program calculation takes about 15 seconds. Given lower computational costs and slight differences with numerical simulations, the proposed method can be considered an efficient tool for the preliminary design of convex slopes.

However, for the case of concave slopes, it can be seen from Figure 6(b) that there is a relatively significant difference between the proposed method and the numerical results, and the difference is basically between 25% and 35%. We think that the large error is due to the fact that when the concave slope reaches the limit equilibrium state, compression between soil slices will lead to an increase of the lateral stress on both sides of each soil slice, and the Rankine active earth pressure will lead to a smaller value at this time. Therefore, whether the proposed method is suitable for concave slope stability analysis remains to be evaluated in the future.

4. Discussion

4.1. Influence of Lateral Stress Reduction. It has been emphasized that the attribute of lateral pressures among neighboring soil columns in the stability analyses of concave and convex slopes in Section 2. However, there is no knowledge about whether the strength reduction should be accounted for when calculating the lateral stress on soil slices. Therefore, it is necessary to clarify this point, helping to have a deeper understanding of the limit equilibrium stability analyses of concave and convex slopes. Figure 7 compares the FS between the limit equilibrium analyses with and without considering the strength reduction in computing the lateral stresses on soil slices where the input parameters are: $H = 10$ m, $\gamma = 20$ kN/m^3, and $R = 10$ m.

It can be seen from Figure 7(a) that whether the lateral stress should be reduced or not has a significant impact on the FSs of convex slopes. When the slope angle is 60° and the soil cohesion c is less than 15 kPa, the difference between the cases of considering and neglecting strength reduction in calculating the lateral stress on soil slices is less than 5%, but such difference increases gradually with increasing the soil cohesion c. When the soil cohesion c is up to 30 kPa, the difference attains up to 15%. Comparatively, when the slope angle is 70°, the FSs calculated without lateral stress reduction are lower than those calculated by the proposed method, and the difference decreases with the increases of the frictional angle of soils φ where the maximum difference reaches 25%. Such a comparison implies that the calculation of the lateral stress on soil slices should be carefully checked in engineering practice when the limit equilibrium analysis is conducted for the stability analysis of a convex slope. For concave slope, as shown in Figure 8(b), the comparison results show that the FSs calculated without lateral pressure reduction are close to and less than their counterpart. Such results indicate that whether lateral stress is reduced or not has little effect on concave slope's FS.

4.2. Influence of Slip Lines in the Two-Dimensional Space. The main novelty of this study lies in proposing a slip surface that can be generated automatically by satisfying the kinematic constraint. Aimed to demonstrate the advance of the proposed slip surface, a comparison with the conventional circular slip line in the two-dimensional space is performed in terms of FSs. Based on the stress analysis method of soil slices in Section 2.2, the formula for calculating the FSs when the slip surface in the two-dimensional space is circular and logarithmic spiral can be easily derived. For this reason, the detailed derivations are not given herein. Figure 9 shows the comparison results of FSs as a function of c at $H = 10$ m, $\gamma = 20$ kN/m^3, and $R = 10$ m.

For convex slopes, according to Figure 8(a), when a circular slip line is used, the FS is close to the numerical result and is higher than that calculated by the slip surface generated by the discretization technology. That is to say, the proposed model produces conservative estimates, and using the circular slip line may lead to unsafe results in the case of convex slopes. At the same time, when a logarithmic spiral is used, the FS is very close to the results calculated by the slip surface generated by the discretization technology. With the increase of φ, the difference between using a circular slip line, using a discrete slip line, and using a logarithmic spiral decreases. Although the comparison results of FSs show that the results of using a circular slip line are closer to those of

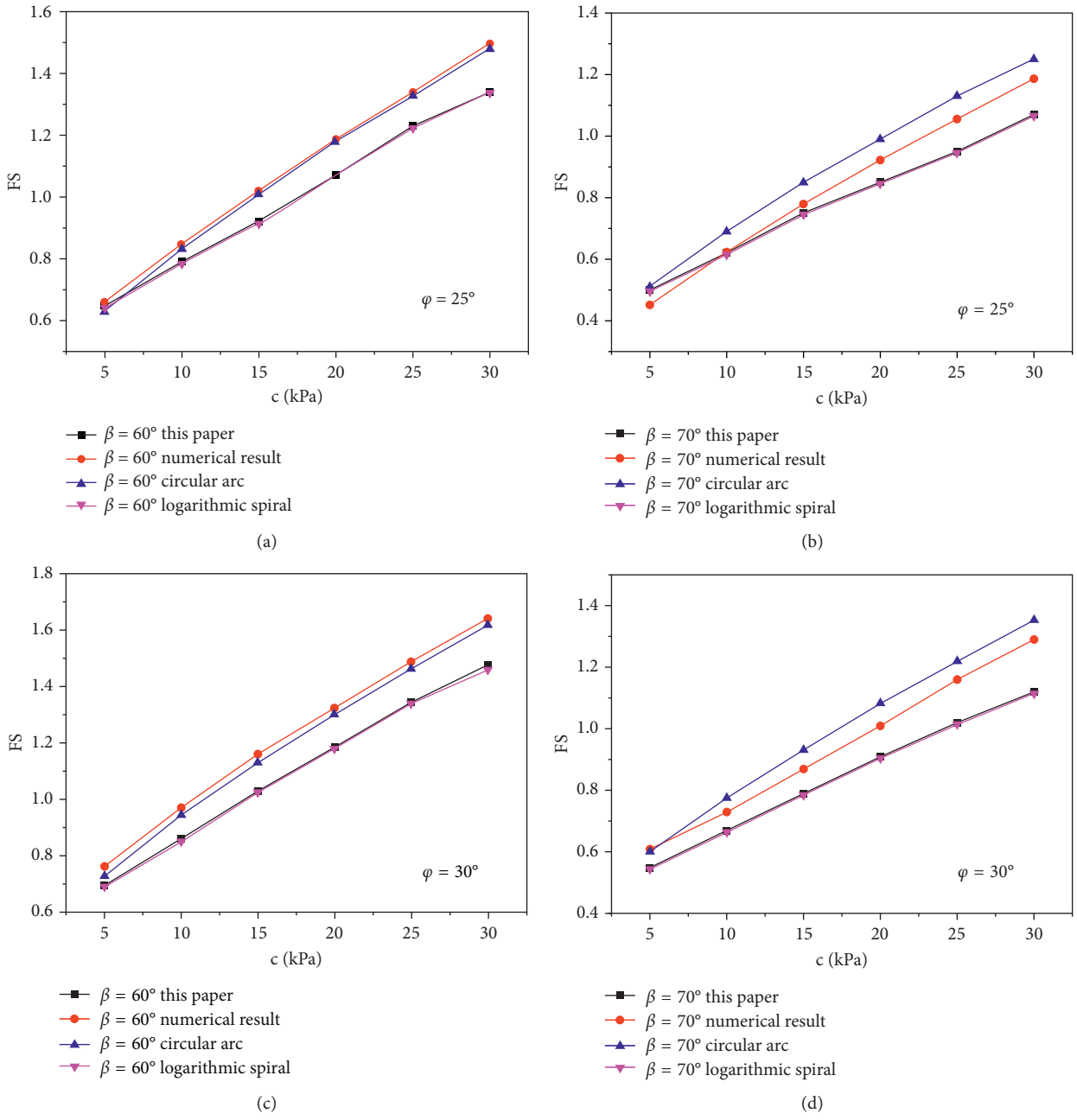

Figure 8: Continued.

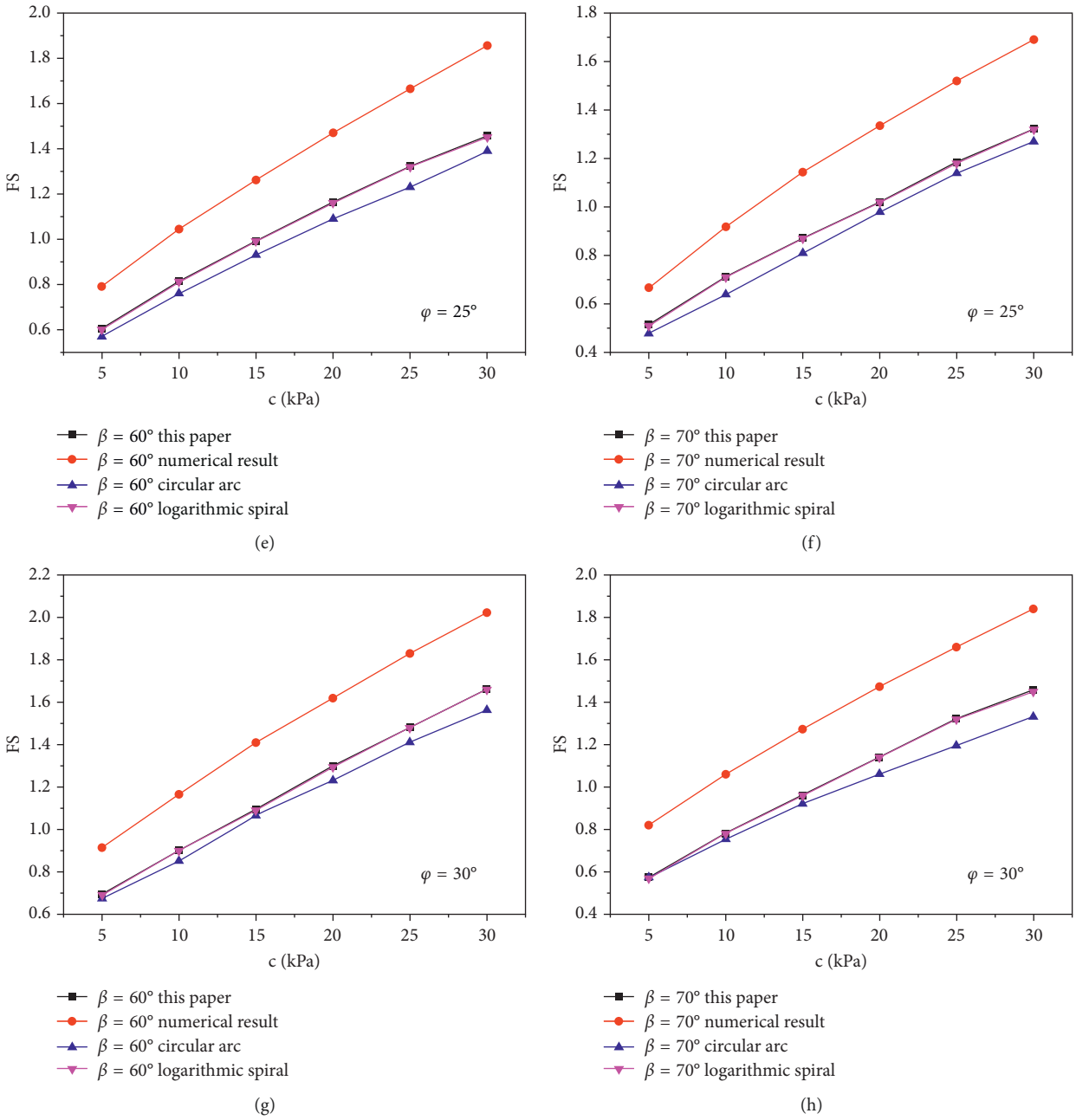

Figure 8: Comparison of FS: (a)–(d) convex slope and (e)–(h) concave slope.

numerical models compared with using the proposed slip line and using a logarithmic spiral, the slip line generated by discretization technology is more similar to that generated by the numerical model and logarithmic spiral, as can be seen in Figure 9. As for concave slope, as shown in Figure 8(b), the FS calculated by using circular slip lines is close to those by the proposed model using the "point-by-point" technique and those by using logarithmic spirals. However, like the comparison between FLAC3D results and the results obtained by the proposed method, the results calculated by circular arc slip surface; the results calculated by logarithmic spiral slip surface also greatly differ from FLAC3D results; and the difference increases with the increase of the soil cohesion c. As shown in Figure 9, although there is a significant difference between the FSs obtained by the developed method and that obtained by the numerical model, it can be found that the shape of the slip surface generated by the discretization technology is consistent with that generated by the numerical model and logarithmic spiral slip surface.

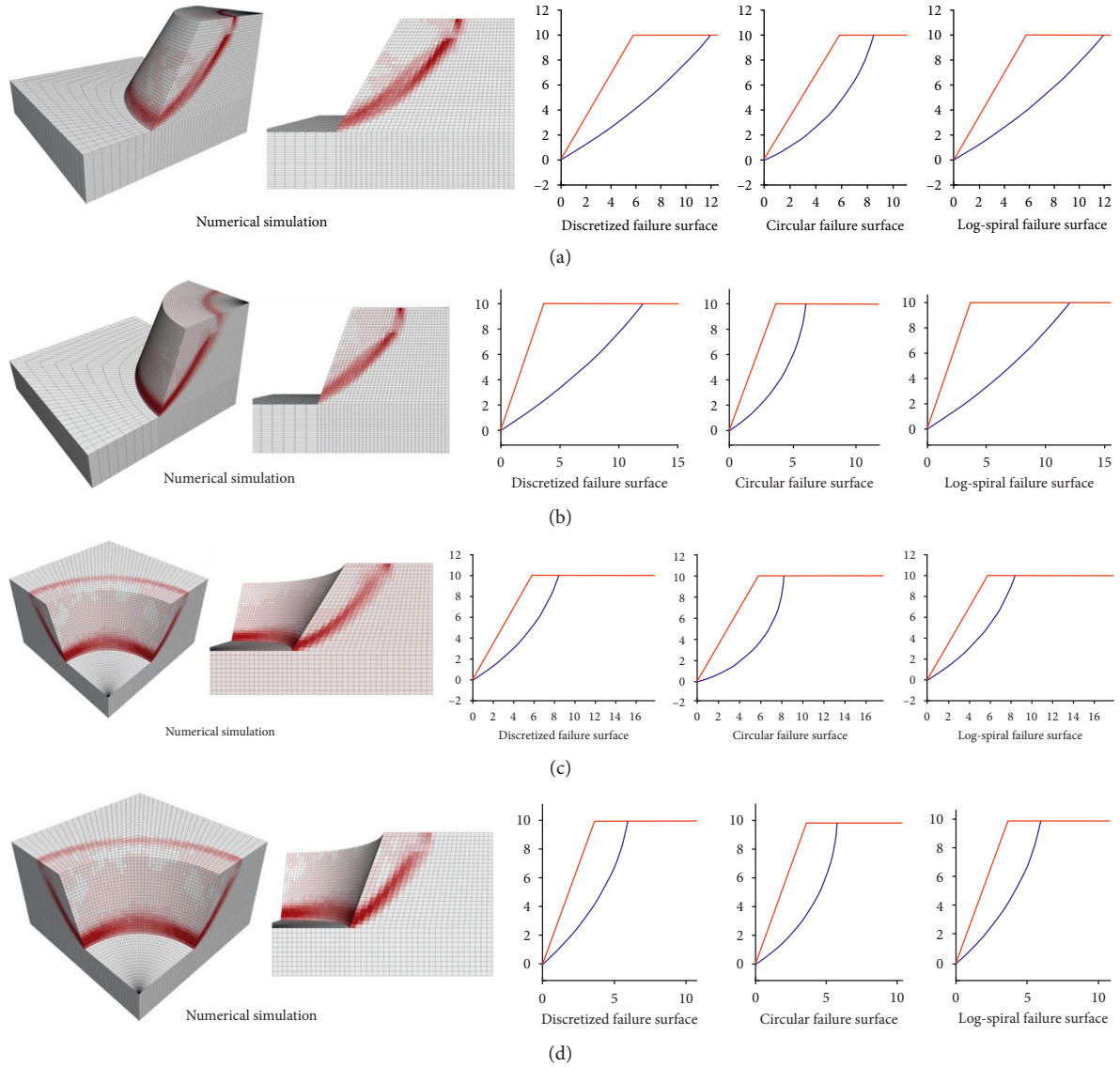

FIGURE 9: Shape of slip surface ($H = 10\,\text{m}$, $\gamma = 20\,\text{kN/m}^3$, $c = 20\text{kPa}$; $\varphi = 30^\circ$): (a) convex slope, $\beta = 60^\circ$; (b) convex slope, $\beta = 70^\circ$; (c) concave slope, $\beta = 60^\circ$; and (d) concave slope, $\beta = 70^\circ$.

5. Conclusions

This work investigates convex slope and concave slope stability by means of the limit equilibrium method combined with the discretization technology and the simplified Bishop method. The three-dimensional failure mechanism of convex and concave slopes subjected to rotational failure is constructed with the aid of the forward difference "point-by-point" technique where the kinematic constraint is satisfied. The three-dimensional vertical slice method is employed to construct the balanced formula of forces and moment concerning the failure body of convex and concave slopes where Rankine's theory is employed to derive the lateral pressure on soil slices. The FSs of slopes are implicitly obtained based on the strength reduction method, which compares well with the finite difference numerical simulation.

Through the research of this paper, we can draw the following conclusions:

(1) Comparisons with the numerical analysis results (FLAC3D) show that the derived formula can effectively evaluate the convex slope stability. Comparatively, there is a relatively significant difference between the proposed method and the numerical results for the case of concave slopes. This is because when the concave slope reaches the limit equilibrium state, compression between soil slices will lead to an increase in the lateral stress on both sides of each soil slice.

(2) The lateral force on three-dimensional neighboring soli slices can be simplified to the Rankine active earth force, and the strength reduction should be

made when calculating the lateral stress on neighboring soil slices.

(3) Compared with the method using the conventional circular slip surface, the shape of the slip surface generated by the discretization technology is closer to that calculated by the numerical model, demonstrating the significance of taking kinematic constraint into account. At the same time, when the slope is homogeneous, the discretized slip surface can degenerate into a logarithmic spiral. Especially, for convex slopes, the conventional method neglecting kinematic constraint may predict unsafe results, which should be carefully checked in engineering practice.

Data Availability

All data, models, or codes that support the findings of this study are available from the corresponding author upon reasonable request.

Conflicts of Interest

The authors declare that they have no conflicts of interest.

Acknowledgments

This work was supported by the Chinese Railway Si-Yuan Survey and Design Group R & D Plan (2020K045-1).

References

[1] D. R. Piteau and J. E. Jennings, "The effects of plan geometry on the stability of natural slopes in rock in the Kimberley area of South Africa," in *Proceedings of the 2nd Congress of the International Society of Rock Mechanics*, no. 3, pp. 7–4, Belgrade, Yugoslavia, June 1970.

[2] E. Hoek and J. D. Bray, *Rock Slope Engineering*, CRC Press, Florida, FL, USA, 1981.

[3] K. L. Lu and D. Y. Zhu, "Theoretical and experimental study of effect of slope topography on its stability," *Chinese Journal of Rock Mechanics and Engineering*, vol. 33, no. 1, pp. 35–42, 2014.

[4] L. Lorig, "Lessons learned from slope stability studies," in *FLAC and Numerical Modeling in Geomechanics*, pp. 17–21, CRC Press, Florida, FL, USA, 2020.

[5] M. Cała, "Convex and concave slope stability analyses with numerical methods," *Archives of Mining Sciences*, vol. 52, no. 1, pp. 75–89, 2007.

[6] C. Sun, J. Chai, Z. Xu, and Y. Qin, "3D stability charts for convex and concave slopes in plan-view with homogeneous soil based on the strength-reduction method," *International Journal of Geomechanics*, vol. 17, no. 5, Article ID 06016034, 2017.

[7] A. Johari, S. Mousavi, and A. Hooshmand Nejad, "A seismic slope stability probabilistic model based on Bishop's method using analytical approach," *Scientia Iranica*, vol. 22, no. 3, pp. 728–741, 2015.

[8] A. Johari and S. Mousavi, "An analytical probabilistic analysis of slopes based on limit equilibrium methods," *Bulletin of Engineering Geology and the Environment*, vol. 78, no. 6, pp. 4333–4347, 2019.

[9] Z. Xing, "Three-dimensional stability analysis of concave slopes in plan-view," *Journal of Geotechnical Engineering*, vol. 114, no. 6, pp. 658–671, 1988.

[10] T. Zhang, Q. Cai, L. Han, J. Shu, and W. Zhou, "3D stability analysis method of concave slope based on the Bishop method," *International Journal of Mining Science and Technology*, vol. 27, no. 2, pp. 365–370, 2017.

[11] Y. M. Cheng and C. K. Lau, *Slope Stability Analysis and Stabilization: New Methods and Insight*, CRC Press, Florida, FL, USA, 2008.

[12] J. Konkol, "Selected aspects of the stability assessment of slopes with the assumption of cylindrical slip surfaces," *Computers and Geotechnics*, vol. 37, no. 6, pp. 796–801, 2010.

[13] Y. C. Yang, H. G. Xing, X. G. Yang, and J. W. Zhou, "Determining the critical slip surface of three-dimensional soil slopes from the stress fields solved using the finite element method," *Mathematical Problems in Engineering*, vol. 2016, pp. 1–11, Article ID 7895615, 2016.

[14] R. Kalatehjari, A. Arefnia, A. S. A Rashid, N. Ali, and M. Hajihassani, "Determination of three-dimensional shape of failure in soil slopes," *Canadian Geotechnical Journal*, vol. 52, no. 9, pp. 1283–1301, 2015.

[15] G. Mollon, K. K. Phoon, D. Dias, and A. H. Soubra, "Validation of a new 2D failure mechanism for the stability analysis of a pressurized tunnel face in a spatially varying sand," *Journal of Engineering Mechanics*, vol. 137, no. 1, pp. 8–21, 2011.

[16] G. Mollon, D. Dias, and A. H. Soubra, "Rotational failure mechanisms for the face stability analysis of tunnels driven by a pressurized shield," *International Journal for Numerical and Analytical Methods in Geomechanics*, vol. 35, no. 12, pp. 1363–1388, 2011.

[17] Q. Pan and D. Dias, "The effect of pore water pressure on tunnel face stability," *International Journal for Numerical and Analytical Methods in Geomechanics*, vol. 40, no. 15, pp. 2123–2136, 2016.

[18] C. Qin and S. C. Chian, "Bearing capacity analysis of a saturated non-uniform soil slope with discretization-based kinematic analysis," *Computers and Geotechnics*, vol. 96, pp. 246–257, 2018.

[19] C. Qin and S. C. Chian, "Impact of earthquake characteristics on seismic slope stability using modified pseudodynamic method," *International Journal of Geomechanics*, vol. 19, no. 9, Article ID 04019106, 2019.

[20] G. H. Chen, J. F. Zou, Q. J. Pan, Z. H. Qian, and H. Y. Shi, "Earthquake-induced slope displacements in heterogeneous soils with tensile strength cut-off," *Computers and Geotechnics*, vol. 124, Article ID 103637, 2020.

[21] Z. H. Qian, J. F. Zou, J. Tian, and Q. J. Pan, "Estimations of active and passive earth thrusts of non-homogeneous frictional soils using a discretisation technique," *Computers and Geotechnics*, vol. 119, Article ID 103366, 2020.

[22] Z. H. Qian, J. F. Zou, Q. J. Pan, G. H. Chen, and S. X. Liu, "Discretization-based kinematical analysis of three-dimensional seismic active earth pressures under nonlinear failure criterion," *Computers and Geotechnics*, vol. 126, Article ID 103739, 2020.

[23] Z. H. Qian, J. F. Zou, and Q. J. Pan, "3D discretized rotational failure mechanism for slope stability analysis," *International Journal of Geomechanics*, vol. 21, no. 11, Article ID 04021210, 2021.

[24] Z. H. Qian, X. X. Wei, Q. Huang, and J. F. Zou, "Earth pressure estimation of undrained soil–wall systems with head

rotation," *International Journal of Geomechanics*, vol. 22, no. 6, Article ID 04022081,, 2022.
[25] Z. H. Qian and J. F. Zou, "Three-dimensional rigorous upper-bound limit analysis of soil slopes subjected to variable seismic excitations," *Computers and Geotechnics*, vol. 147, Article ID 104714, 2022.
[26] G. H. Chen, J. F. Zou, X. Y. Xiang, Q. J. Pan, and Z. H. Qian, "Stability assessments of reinforced tunnel face using improved homogenization approach," *International Journal of Geomechanics*, vol. 21, no. 10, Article ID 04021183, 2021.
[27] J. Zou, G. Chen, and Z. Qian, "Tunnel face stability in cohesion-frictional soils considering the soil arching effect by improved failure models," *Computers and Geotechnics*, vol. 106, pp. 1–17, 2019a.
[28] J. F. Zou, Z. H. Qian, X. H. Xiang, and G. h. Chen, "Face stability of a tunnel excavated in saturated nonhomogeneous soils," *Tunnelling and Underground Space Technology*, vol. 83, pp. 1–17, 2019b.
[29] M. Cala and J. Flisiak, "Slope stability analysis with FLAC and limit equilibrium methods," in *FLAC and Numerical Modeling in Geomechanics*, pp. 111–114, CRC Press, Florida, FL, USA, 2020.
[30] Y. M. Cheng, T. Lansivaara, and W. B. Wei, "Two-dimensional slope stability analysis by limit equilibrium and strength reduction methods," *Computers and Geotechnics*, vol. 34, no. 3, pp. 137–150, 2007.